ACS APPLIED MATERIALS & INTERFACES

Research Article

www.acsami.org

Hierarchical Nanogaps within Bioscaffold Arrays as a High-Performance SERS Substrate for Animal Virus Biosensing

Feng Shao,[†] Zhicheng Lu,[†] Chen Liu,[†] Heyou Han,*[,†] Kun Chen,[†] Wentao Li,[‡] Qigai He,[‡] Hui Peng,[†] and Juanni Chen[†]

[†]State Key Laboratory of Agricultural Microbiology, College of Science, Huazhong Agricultural University, Wuhan 430070, China

[‡]State Key Laboratory of Agricultural Microbiology, College of Animal Science and Veterinary Medicine, Huazhong Agricultural University, Wuhan 430070, China

Supporting Information

ABSTRACT: A three-dimensional (3D) biomimetic SERS substrate with hierarchical nanogaps was formed on the bioscaffold arrays of cicada wings by one-step and reagents-free ion-sputtering techniques. This approach requires a minimal fabrication effort and cost and offers Ag nanoislands and Ag nanoflowers with four types of nanogaps (<10 nm) on the chitin nanopillars to generate a high density of hotspots (~2000/μm^2). The 3D biomimetic substrate shows a low detection limit to Rhodamine 6G (10^{-13} M), high average enhancement factor (EF, 5.8×10^7), excellent signal uniformity (5.4%), good stability, and suitability in biosensing. Furthermore, the finite-difference time-domain (FDTD) electric-field-distribution simulations illustrate that the 3D biomimetic SERS substrate provides the high-density hotspot area within a detection volumem, resulting in enormous SERS enhancement. In addition, the conspicuous far-field plasmon resonance peaks were not found to be a strong requirement for a high EF in 3D biomimetic substrates. Additionally, the novel substrate was applied in label-free animal viruses detection and differentiation with small amounts (1.0 μL) and low concentrations of analyte (1×10^3 PFU/mL), and it exhibited potential as an effective SERS platform for virus detection and sensing.

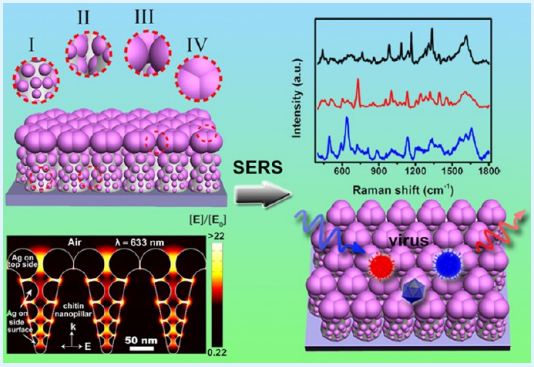

KEYWORDS: *3D biomimetic SERS substrate, hotspots, nanogaps, cicada wings, label-free virus detection*

INTRODUCTION

Surface-enhanced Raman scattering (SERS) is the phenomenon whereby Raman signals are strongly increased when molecules are attached to nanorough metallic structures.[1] With its integration of high sensitivity, rapid response, noninvasive analysis, and fingerprint effect,[2−5] SERS spectroscopy has become one of the most vibrant analytical tools for chemical and biological sensing. It has been established that large SERS enhancements are normally associated with the enormously intensified electromagnetic (EM) fields at hotspots created by the strong coupling of localized surface plasmon resonances (LSPR) at interstitial junctions or nanogaps between metallic nanostructures.[6] To date, a great deal of effort has been devoted to the development of SERS substrates having the desired density, sensitivity, and reproducibility of hotspots within diverse plasmonic structures to give the strongest possible SERS signal.[7] However, achieving a large-scale fabrication of SERS substrates with a high density of hotspots by straightforward and cost-effective routes still remains a challenge, thus limiting the widespread adoption of SERS as a general sensing technique.

General approaches to fabricating one-dimensional (1D) nanogaps for SERS hotspots are based on the aggregation of colloidal plasmonic nanoparticles (NPs), where these hotspots are random in dimension, quantity, and location by nature.[8] Other conventional methods for generating two-dimensional (2D) nanogap structures with vertical homogeneity and suitable reproducibility mainly include lithography techniques,[9,10] Langmuir−Blodgett assembly,[11] and nanoparticle self-assembly.[12−14] These planar substrates, however, remain modest in sensitivity because of the limited concentration of hotspots available within the detection volume.[15] In contrast, three-dimensional (3D) substrates offer the advantage of a greater number of hotspots and binding sites for probing molecules within the laser footprint.[16] Emerging 3D SERS substrates have been fabricated by 3D assembly[17,18] as well as by decorating noble-metal NPs onto nanoscaffolds, including nanocanals,[19] nanowires,[20] nanopillars,[21,22] nanorods,[23,24] and carbon nanotube[7,25] arrays. Nevertheless, the indispensable preparations of these scaffolds are cumbersome and time-consuming, thus increasing the cost of fabrication and the difficulty of accessibility. Recently, Stoddart et al.[26] and Garrett

Received: October 14, 2013
Accepted: December 20, 2013
Published: December 20, 2013

dx.doi.org/10.1021/am4045212 | ACS Appl. Mater. Interfaces 2014, 6, 6281−6289

et al.[27] proposed an alternative manufacturing technique, biomimetic SERS substrates based on the chitin bioscaffold, to explore an interesting approach to fabricate SERS substrates. Despite the attractivity of the bioscaffolds, these available biomimetic SERS substrates are still confined to 2D structures and remain to be further rationally designed for the expansion of their expected potential.

In this work, we report a novel 3D biomimetic SERS substrate with a high density of hotspots, dependable performance, and good reproducibility based on naturally occurring nanostructures. The chitin nanopillar arrays (CNAs) on the cicada (*Cryptotympana atrata Fabricius*), which is a widespread insect that can be artificially cultured, provide a new bioscaffold for decorating with Ag NPs in different dimensions to realize a 3D SERS substrate with multiple sub 10 nm nanogaps by direct-current (dc) ion sputtering. Through this simple physical vapor deposition (PVD) technique without using any reagents, we have elaborately created and regulated hierarchical nanostructures on the CNAs with Ag nanoislands (Ag-NIs) on the side surfaces and Ag nanoflowers (Ag-NFs) on the top ends. Moreover, both experimental spectra and simulation of electric-field distributions confirmed that the 3D nanogeometries with plentiful nanogaps (<10 nm) could generate large SERS enhancements under incident light.[21] To validate further its performance and to explore its potential in practical application, the novel SERS substrate was employed in the label-free detection and differentiation of animal viruses, including porcine circovirus type 2 (PCV2), porcine pseudorabies virus (PRV), and avian influenza virus (AVI) subtype H5N1, which made it a promising candidate for creating a rapid pathogen-monitoring platform for use in biosensing.

RESULTS AND DISCUSSION

The fabrication procedure for 3D Ag-decorated CNAs is illustrated in Figure 1. Briefly, the cicada wings were segmented into small sections after being ultrasonically cleaned. Prior to sputtering, as-pretreated sections were fixed on glass slides as bioscaffolds. Finally, Ag-NPs were decorated onto the natural bioscaffolds by top-view dc ion sputtering. It is worth noting that this clean and green dc sputtering technique[23] could give rise to 3D biomimetic substrates with four types of nanogaps on both the side surfaces and the top ends of the CNAs. Furthermore, the physical sputtering strategy could avoid unnecessary, cumbersome stages in chemical surface modification and coupling that link the metal NPs onto the nanoscaffold but probably cause extra interferential bands in the SERS measurements.[23] In particular, the one-step decoration allows the batch conversion of raw materials into 3D biomimetic substrates in less than 1 h (Figure S1), thereby improving productivity significantly in substrates fabrication. In addition, well-veined, transparent membranous wings of the cicada with a typical length of about 50 mm (Figure S2) have been deemed to be low-cost and seasonally abundant bioscaffolds for SERS work.[26,28] When compared with glass,[21] gold,[29] silicon[30] nanopillar, and ZnO[23] nanorod arrays, our study can achieve cost-effective (<$1/piece) and straightforward fabrication of substrates by utilizing CNAs directly as bioscaffolds, and it can increase dramatically substrates affordability and can even improve the SERS EF by at least one order of magnitude compared to the common commercial SERS substrate (Klarite) produced with lithographic techniques.

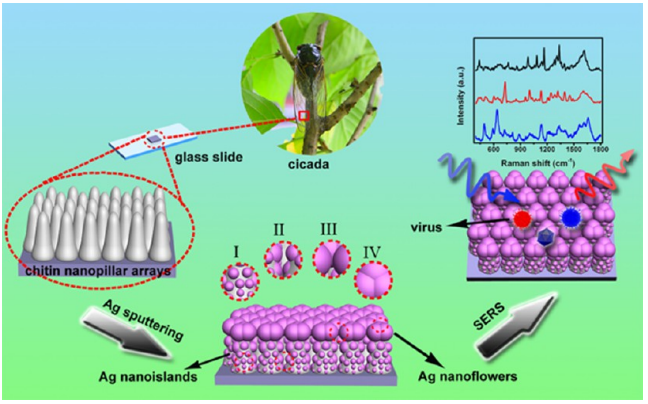

Figure 1. Fabrication process for Ag-decorated CNAs as the 3D biomimetic substrate applied in label-free animal virus detection. Through sputtering, Ag-NIs and Ag-NFs are formed simultaneously on the side surfaces and top ends of chitin nanopillars with hierarchical nanogaps, respectively. There are four types of nanogaps between the Ag-decorated chitin nanopillars to form 3D hotspots, indicated as I, II, III, and IV. Type I has nanogaps between the Ag-NIs located on the side surfaces of single chitin nanopillars, type II has nanogaps between the Ag-NIs located on the side surfaces of the adjacent chitin nanopillars, type III has nanogaps within the Ag-NFs located on the top ends of the adjacent chitin nanopillar, and type IV has nanogaps between the Ag-NFs located on the top ends of the single chitin nanopillars.

For protecting CNAs from damage during sputtering, we rationally decorated quasi-periodic CNAs with Ag NPs by dc sputtering using a 1 min duration followed by a 1 min break. Significantly, the SEM results (Figure S3) indicate that intermittent Ag sputtering could create more Ag-NIs than persistent sputtering under the same conditions, resulting in a 7-fold enhancement in the SERS signal of Rhodamine 6G (R6G, 1 μM) at the 1650 cm^{-1} shift (Figure 2). By adjusting

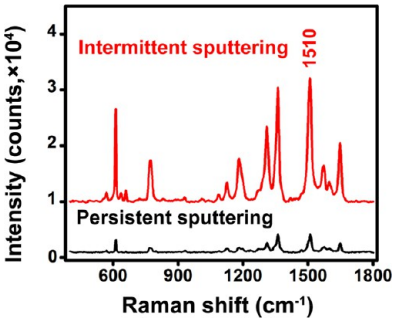

Figure 2. Comparison of SERS spectra of R6G from 3D Ag-decorated CNAs with 10 min intermittent and persistent sputtering.

the ion current and vacuum during sputtering (Figure S3), the Ag-NIs and Ag-NFs with different Ag thickness could be formed simultaneously on the side surfaces and top ends of CNAs. In this case, a thin Ag NPs layer was formed in the fashion of Ag-NIs and Ag-NFs owing to the Volmer–Weber (VW) growth mode, leading to the formation of 3D adatom clusters or islands along with their coarsening on the substrate surface.[31,32] On the basis of a recent study concerning cone-shaped ZnO nanorods,[23] the distinctive morphology can facilitate the sputtering of a large number of Ag-NPs onto the CNAs for 3D geometries generation. As depicted in Figure S2, CNAs are thick at the bottom edge and thin at the top.

dx.doi.org/10.1021/am4045212 | ACS Appl. Mater. Interfaces 2014, 6, 6281–6289

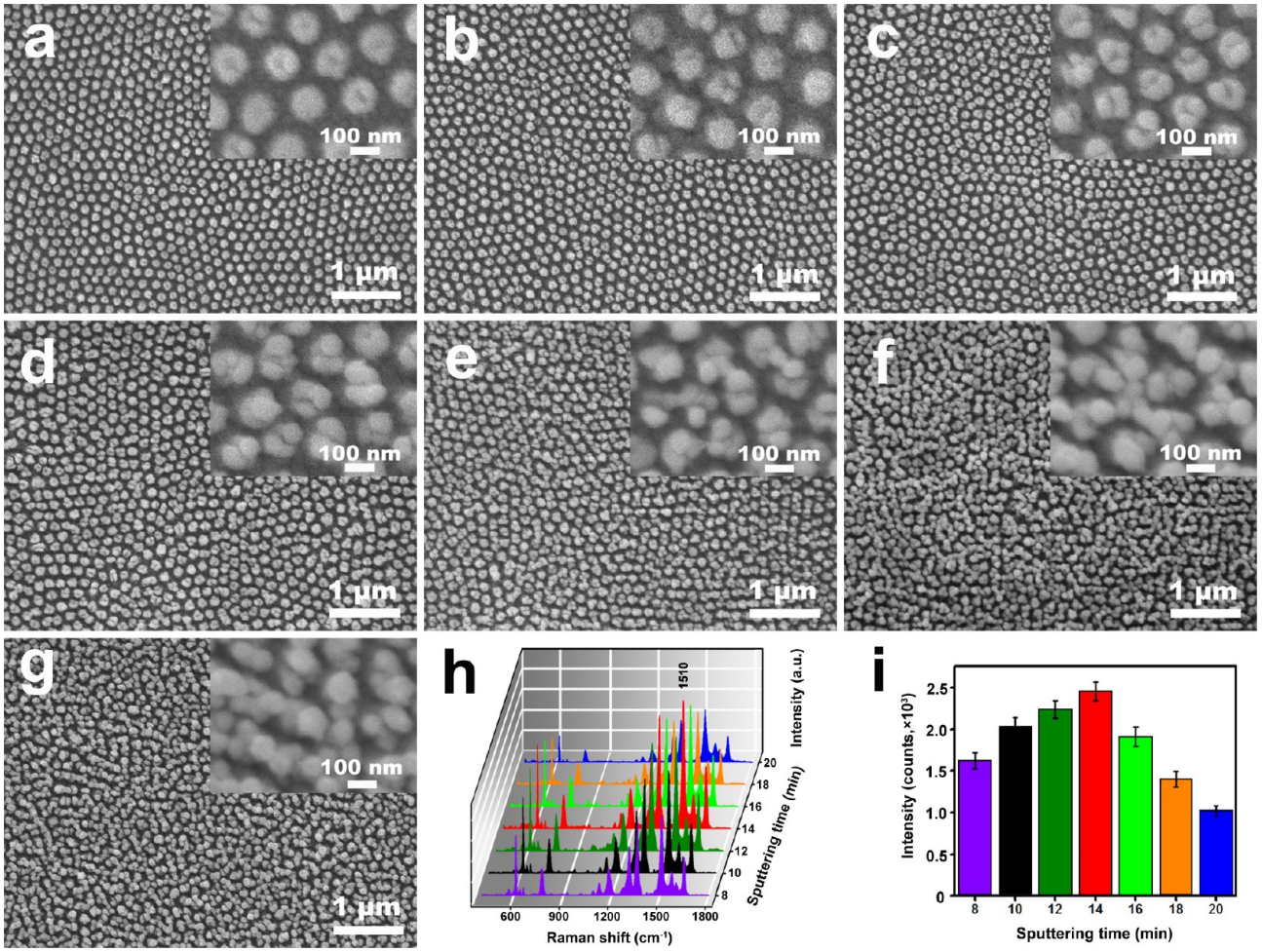

Figure 3. (a–g) Top-view SEM images of 3D biomimetic substrates with a sputtering deposition time range from 8 to 20 min at an interval of 2 min under the same deposition conditions. (h) SERS spectra of R6G (1 μM) molecules absorbed on corresponding SERS substrates under 633 nm laser excitation with an output power of 0.2 mW. (i) Comparison of average Raman intensities at that 1510 cm^{-1} peak on the corresponding substrates.

Furthermore, Figure S2 also reveals that the interstitial region between closely spaced chitin nanopillars, wide at the top and narrow at the bottom, could allow the formation of more Ag-NIs on the side surfaces to facilitate the construction of 3D nanogeometries during sputtering rather than the direct configuration of caps on the tops to obstruct further formation of Ag-NIs. Moreover, Fourier transform infrared spectroscopy (FTIR) indicates that rich amino and hydroxyl groups exist on the surface of the CNAs (Figure S4). Additionaly, high-resolution transmission electron microscopy (HRTEM) images reveal that Ag NPs may tend to combine the (111) plane[23] with the surface of the CNAs (Figure S5). Accordingly, compared with the reported glass,[21] gold,[29] and silicon[30] nanopillar arrays, the unique nanoarchitectures formed with intermittent sputtering techniques and in particular their surface chemical environments contribute to the higher density of 3D nanogaps on the quasi-periodic CNAs within the unit area.[23]

Under selected sputtering conditions, a series of substrates were prepared by applying a sputtering deposition time (DT) from 8 to 20 min at an interval of 2 min (Figure 3). The variation of the SERS intensity of R6G (1 μM) at the 1650 cm^{-1} shift could be ascribed to the particular structural development of the substrates. Before DT reached 14 min, the SERS intensity of R6G increased gradually with decreased spacing between different Ag-NIs and Ag-NFs. For substrates with short sputtering duration (8 min), only a few efficient type I nanogaps could be observed in substrates, resulting in a modest SERS activity. With an extension in the sputtering DT (14 min), both the number and the size of the Ag-NPs increased, leading to a boost in type I nanogaps and the emergence of type II, III, and IV nanogaps. These four types of nanogaps contribute to the higher SERS intensity when abridged to sub 10 nm nanogaps. With a further prolongation of the sputtering DT (20 min), a large portion of the nanostructures were filled with big aggregated Ag NPs, giving rise to a decrease in the density of effective nanogaps (mainly types I and II) and a significant SERS reduction (Figure 3). These results demonstrate that SERS enhancements are affected by both the distances and the density of nanogaps within the laser footprint on substrates.[33,34]

For evaluating spot-to-spot reproducibility, the 3D biomimetic SERS substrates (14 min) were functionalized with 1 μM R6G and Raman-mapped using steps of 20 μm and a laser spot diameter of 2 μm, where each pixel represents the intensity of the Raman peak at the spatial position on the substrates. As illustrated in Figure 4a, the intensity of the 1510 cm^{-1} peak from R6G was plotted to demonstrate uniformity across the entire 3D biomimetic substrate. Moreover, to assess the substrate-to-substrate reproducibility further, we measured SERS signals of R6G at 50 randomly chosen spots from 10

dx.doi.org/10.1021/am4045212 | ACS Appl. Mater. Interfaces 2014, 6, 6281–6289

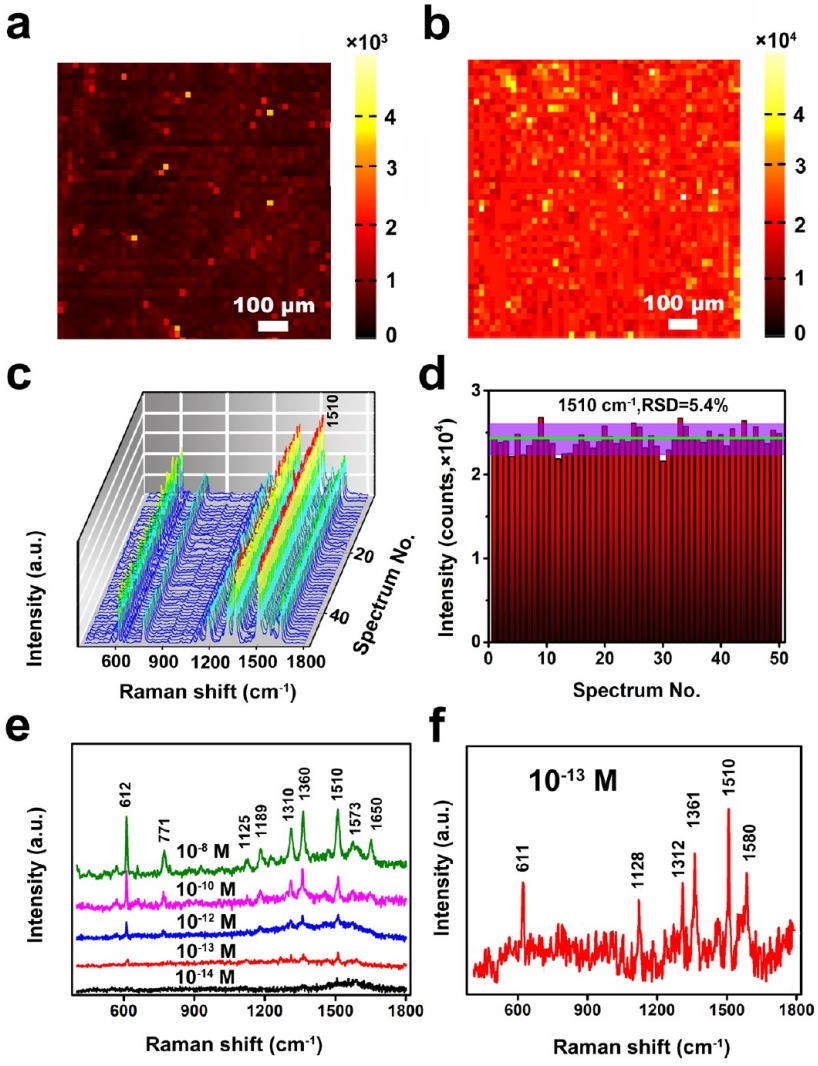

Figure 4. Reproducibility of Klarite and 3D biomimetic substrate (14 min). (a) SERS intensity distribution map of R6G measured at the 1510 cm^{-1} peak across a 1 × 1 mm^2 piece of Klarite and (b) 3D biomimetic substrate. (c) SERS spectra of R6G obtained at 50 spots randomly chosen from 10 3D biomimetic substrates and (d) intensity distribution of the peaks at 1510 cm^{-1} in panel c. The average intensity is indicated with a green line, and the violet zones represent ±5% intensity variation. (e) SERS of R6G solutions in various concentrations using 3D biomimetic substrate. (f) SERS of a 10^{-13} M R6G solution collected on the same substrate with three data accumulations. All substrates were immersed in an R6G (1 μM) aqueous solution for 30 min and measured under 633 nm laser line excitation with an output power of 0.2 mW after rinsing with ultrapure water and drying in air.

3D biomimetic substrates, as shown in Figure 4b. To obtain a statistically meaningful result, the relative standard deviation (RSD) of the intensity at the 1510 cm^{-1} peak of R6G was calculated to be 5.4%, as shown in Figure 4c, which is comparable to[35,36] or even better than many those reported in recent studies.[21,30,37] As shown in Figure 4e,f, the spectral feature characteristics of R6G even at a low concentration of 10^{-13} M could still be identified clearly. Additionally, unlike exposure to the ambient environment, no significant degradation was observed from 3D biomimetic substrates after 4 weeks of storage under vacuum dry conditions (Figure S6).

By regulating dc sputtering, we could conveniently fabricate not only 3D Ag-decorated CNAs with Ag-NIs and Ag-NFs but also 2D Au-capped and 2D Ag-capped CNAs as SERS-active substrates (Figure 5). According to scanning electron microscope (SEM) observations, the electric-field distributions calculated by finite-difference time domain (FDTD) show clearly that a high density of hotspots reside in 3D Ag-decorated CNAs (14 min) under 633 nm excitation, where the hotspots correspond to the locations of the four types of nanogaps. As is known, the EM enhancements of Raman scattering are theoretically predicted to be proportional to $[E]/[E_0]$;[4] hence, the FDTD simulation value of $[E]/[E_0]$ of over 22 indicates that the contribution of EM enhancements to the total EF surpasses 2×10^5.[38] Likewise, 3D Ag-decorated CNAs have hotspots with a dramatically higher density than 2D Au- or Ag-capped CNAs that are similar to the previous work prepared by electron-beam deposition[26] in a detection volume, rendering 3D nanostructures with large SERS enhancements.

The robust SERS enhancements of 3D Ag-decorated CNAs can be attributed to the abundance of the sub 10 nm nanogaps within the unit area, which can result in strong hotspots. Compared to 2D biomimetic substrates, the SEM results show that there are four types of nanogaps within 3D Ag-decorated CNAs but only two types within vertically aligned 2D Au- or Ag-capped CNAs (Figure 5). For 3D Ag-decorated CNAs (14

dx.doi.org/10.1021/am4045212 | ACS Appl. Mater. Interfaces 2014, 6, 6281−6289

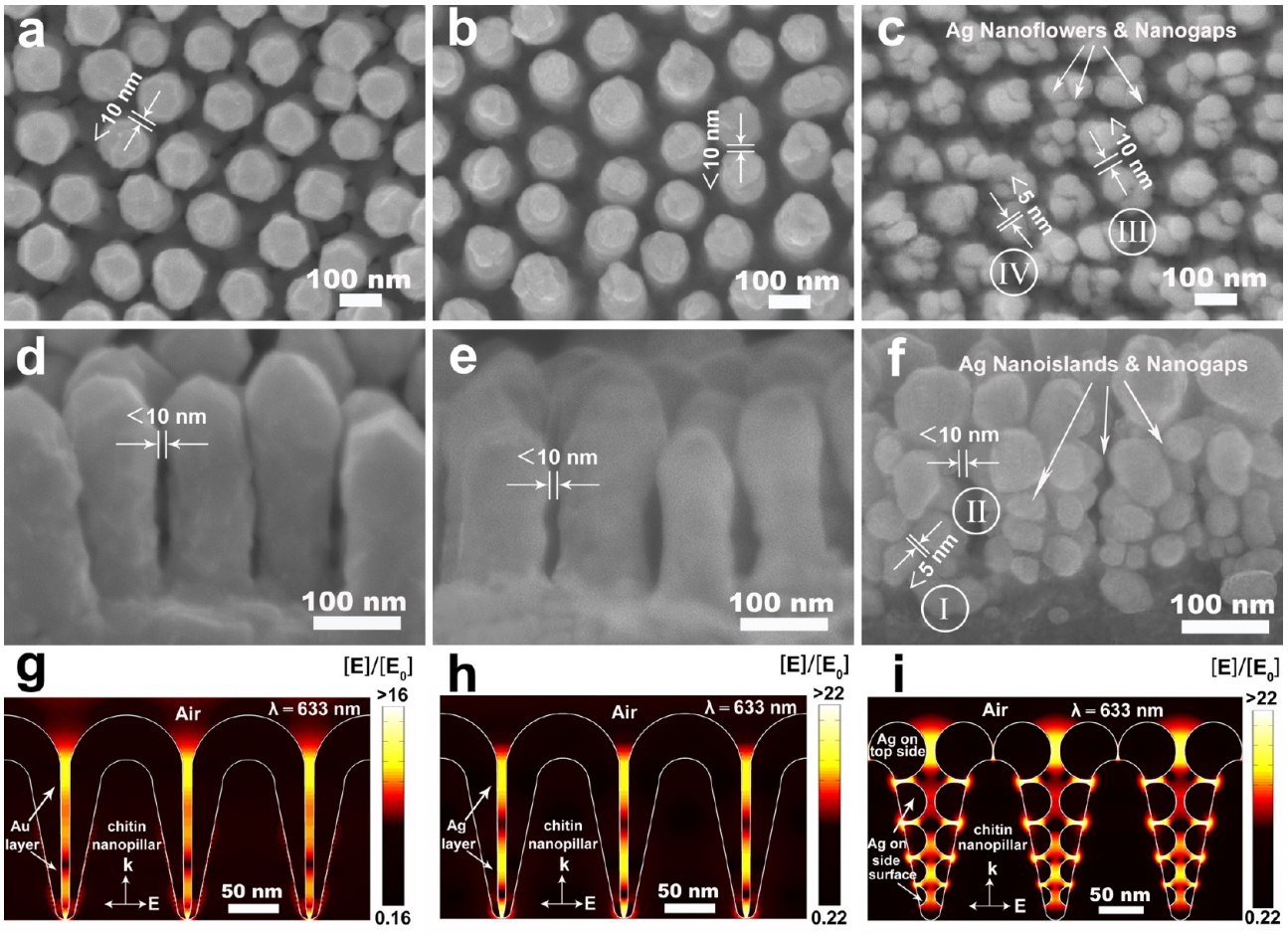

Figure 5. Computer simulations of 2D and 3D biomimetic substrates. (a–c) Top-iew and (d–f) side-view SEM images of 2D Au-capped CNAs, 2D Ag-capped CNAs, and 3D Ag-decorated CNAs with Ag-NIs and Ag-NFs, respectively. (g–i) Finite-difference time-domain (FDTD) computer simulations showing the distribution of electric-field distribution around corresponding substrates. Note that the white lines in the electric-field distribution were added to indicate the boundaries of nanostructures, whereas the white areas represent hotspots with $[E]/[E_0]$ over 22, corresponding to an EF of over 2×10^5.

min), Ag-NFs on the top ends were composed of three big huddled Ag NPs of 50–60 nm in diameter, and Ag-NIs on the side surfaces consisted of small Ag NPs with 20–40 nm diameter (Figure 5c). There are approximately 30 Ag NPs on one individual nanopillar (Figure 5f). Given that there are 35–40 nanopillars within a 1 μm^2 unit (Figure S2), it can be calculated that more than 1000 Ag-NIs exist within 1 μm^2. Consequently, the as-prepared 3D biomimetic substrates can provide nearly 2000 nanogaps (<10 nm), namely, hotspots, within a unit area of 1 μm^2, a much higher density than that reported previously.[22] Moreover, there are a large portion of sub 5 nm nanogaps (types I and IV) in 3D Ag-decorated CNAs, which can further generate enormous SERS enhancements under laser excitation.[33,34]

To achieve vigorous SERS enhancements, we covered 3D Ag-decorated CNAs (14 min) and 2D Au- or Ag-capped CNAs with monolayer benzenethiol (BT) by immersing them for 12 h in a 10 mM BT ethanol solution followed by a rinse with pure ethanol. The mean SERS intensity at the 1578 cm^{-1} peak of monolayer BT with 633 nm laser illumination from the 3D Ag-decorated CNAs was shown to be over one order magnitude higher than that from the 2D capped CNAs and commercial Klarite substrate (Figure 6a). Figure 6b describes the UV–vis diffuse reflectance spectra of the CNAs-based biomimetic and commercial substrates. As can be seen, the reflectance spectra of the Klarite substrate were separated by pronounced reflectivity dips around 570 and 750 nm, which was probably due to the excitation of the LSPR of the gold NPs film.[39] However, similar distinctive reflectivity minima were not observed in the spectra recorded on CNAs decorated with metal NPs and caps. This absence of neat and isolated plasmon resonance is perhaps due to the antireflection structure of the CNAs[26] and the random configuration and distribution of nanogaps. In combination with the elimination effect of plasmon quenching, these nanogaps in 3D biomimetic substrates manifest their application in highly sensitive SERS measurements without a visible plasmon resonance in the far field. Furthermore, Table 1 indicates the average EF as a function of excitation wavelength, and the 3D Ag-decorated CNAs boost the average EF by at least 10-fold over 2D Au- or Ag-capped CNAs and Klarite substrate under different laser illumination. It should be noted that the average EF is calculated by the surface area of the entire 3D Ag-decorated CNAs structure rather than considering only the local surface area at the nanogap. Because the near field likely contributes dominantly to the large SERS EF, the maximum local EF is expected to be even higher than 10^9 within sub 5 nm gap structures (types I and IV), with a spatial-average EF of above

dx.doi.org/10.1021/am4045212 | ACS Appl. Mater. Interfaces 2014, 6, 6281–6289

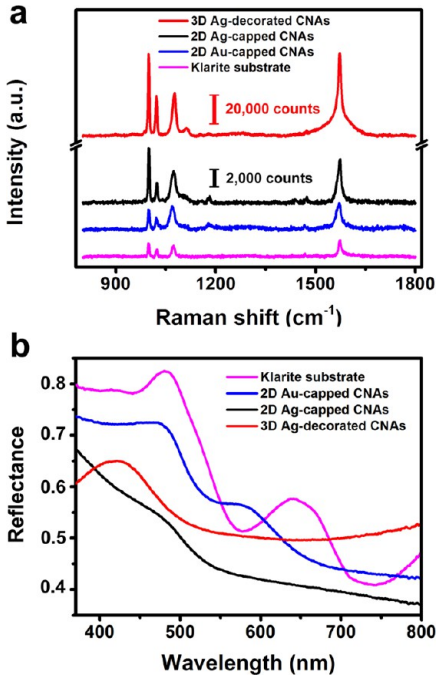

Figure 6. (a) SERS spectra of monolayer benzenethiol and (b) reflectance spectra from different substrates.

Table 1. Average Enhancement Factor of Different Substrates with Three Common Exciting Laser Lines

substrate	514 nm	633 nm	785 nm
3D Ag-decorated CNAs	1.6×10^6	1.2×10^7	5.8×10^7
2D Ag-capped CNAs	1.5×10^5	1.1×10^6	5.0×10^6
2D Au-capped CNAs	9.1×10^4	6.6×10^5	3.6×10^6
Klarite substrate	7.7×10^4	5.1×10^5	1.7×10^6

10^7.[33] Significantly, when the 785 nm laser was employed, the largest average EF (5.8×10^7 with a variation of 5.2%, Table S1) from 3D Ag-decorated CNAs was observed (Table 1), which is a factor of approximately 12, 16, and 34 times higher than that from 2D Ag-capped CNAs, 2D Au-capped CNAs, and Klarite substrate, respectively. Accordingly, 3D Ag-decorated CNAs could serve as a feasible platform for biosensing by excitation with a NIR source, which is desirable for Raman spectroscopy of biological samples to minimize unwanted fluorescence background. In summary, our study has confirmed the possibility of a facile large-scale method for producing a 3D SERS substrate that is suitable for biosensing and can facilitate strong hotspots even without a requirement of far-field plasmon resonance.

To evaluate the sensitivity and reproducibility of the 3D biomimetic substrate in pathogen biosensing, we introduced three kinds of animal viruses with different sizes and surface composition, PCV2, PRV, and H5N1, which are associated with various animal diseases and lead to great financial damage, even threating human health and life.[40−43] PCV2 is an icosahedral, nonenveloped, circular virus of approximately 17 nm in diameter.[44] PRV is an icosahedral virus with a size between 100 and 150 nm and is surrounded by a capsid, envelope, and an 8−10 nm spike.[45] H5N1 is a pleomorphic virus of 80−120 nm in diameter and is composed of a host-derived lipid bilayer envelope in which the virus-encoded glycoproteins HA, neuraminidase (NA), and M2 are embedded.[46] Traditional antibody-based techniques for monitoring viruses, such as enzyme-linked immunosorbent assays (ELISA)[47] and fluoroimmunoassays,[48] have a comparatively low sensitivity and specificity. As an alternative, polymerase chain reaction (PCR) assays tend to be costly and cumbersome. However, the label-free SERS technique allows for rapid, simple, and low-cost virus detection and differentiation.[49]

It can be seen from the three typical SERS spectra of the animal viruses in Figure 7a that the 3D biomimetic substrate could detect and distinguish different complex viral pathogens. In addition, a high degree of reproducibility can be observed in the spectra of the individual viruses obtained on the 3D

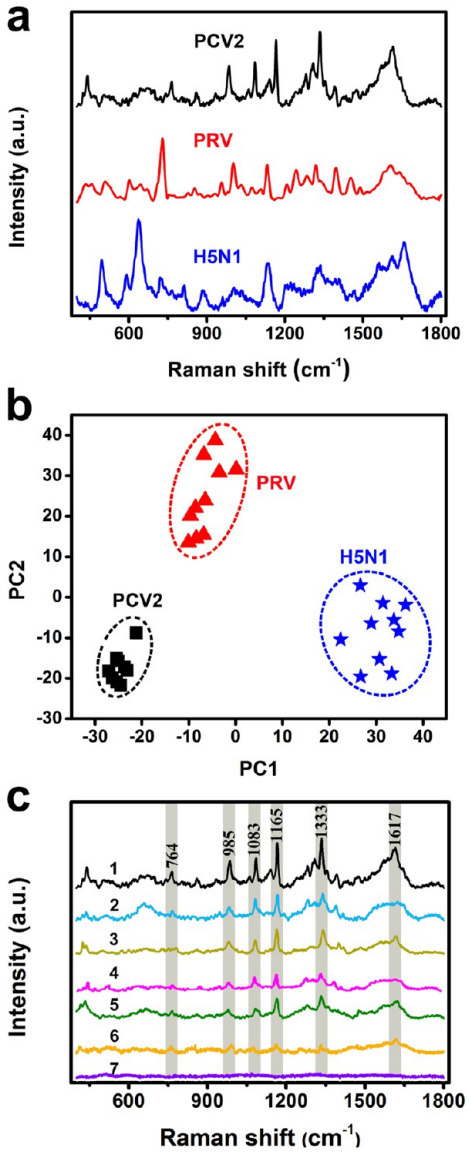

Figure 7. (a) SERS spectra of PCV2, PRV, and H5N1 recorded at the 3D biomimetic substrates. All SERS spectra were excited by the 785 nm laser line with an output power of 25.0 mW and three times of accumulation. Spectra were collected from several spots on multiple substrates and baseline-corrected and smoothed for a clearer view of the spectral differences. (b) Principle components analysis (PCA) plot of PC1 vs PC2 computed from the SERS spectra of PCV2, PRV, and H5N1. (c) SERS spectra of PCV2 on the 3D biomimetic substrate ((1) 10^6 PFU/mL, (3) 10^5 PFU/mL, (5) 10^4 PFU/mL, (6) 10^3 PFU/mL, and (7) ultrapure water) and Klarite substrate ((2) 10^6 PFU/mL and (4) 10^5 PFU/mL) with different concentrations.

dx.doi.org/10.1021/am4045212 | ACS Appl. Mater. Interfaces 2014, 6, 6281−6289

biomimetic substrate in Figure S7. To the best of our knowledge, this is the first report on SERS spectra for the PCV2, PRV, and H5N1 viruses, which could serve as fingerprints for a possible noninvasive diagnosis of animal disease. Figure 7b presents the principal components analysis (PCA) clustering results from the SERS spectra of the PCV2, PRV, and H5N1 viruses, indicating that they are clearly separated into individual clusters, further confirming that the SERS spectra obtained could effectively and reproducibly discriminate these viruses. Additionally, several typical characteristic bands of the PCV2 SERS spectra as low as 1×10^3 PFU/mL were readily detectable on the 3D biomimetic substrate, a detection limit that is about two orders of magnitude lower than that obtained from Klarite substrate (Figure 7c). These bands are most likely due to C−C in-plane bending (764 cm^{-1}), NH_2 in-phase rock and C−O stretch (985 cm^{-1}), C−S stretching vibrations (1083 cm^{-1}), C−N stretching (1165 cm^{-1}), Trp (1333 cm^{-1}), and Tyr and Trp (1617 cm^{-1}), respectively.[50] The results manifest that the 3D biomimetic substrate collaborated with PCA has great potential to detect and differentiate viruses using small amounts and low concentrations of analyte.

CONCLUSIONS

A novel 3D biomimetic SERS substrate inspired from naturally occurring CNAs for label-free animal virus detection was developed. By using CNAs as a bioscaffold, our strategy requires a minimumal fabrication cost and effort and offers great simplicity and fully accessibility for the formation of 3D SERS substrate. With the help of one-step and reagents-free sputtering decoration techniques, Ag-NIs and Ag-NFs were formed simultaneously on the side surfaces and top ends of CNAs, respectively, with four types of nanogaps (<10 nm) to generate a high density of hotspots (~2000/μm^2). Furthermore, in comparison with conventional 2D Au- and Ag-capped CNAs, the FDTD electric-field-distribution simulations intuitively illustrate that the 3D biomimetic SERS substrate increases the hotspots area with a high density within a detection volume. Significantly, apart from its excellent signal reproducibility (5.4%), the resulting substrate also manifests a low detection limit to R6G (10^{-13} M) and high average EF (5.8×10^7), which is at least one order of magnitude higher than that obtained from 2D biomimetic or commercial substrates. In addition, the conspicuous far-field plasmon resonance peaks were not found to be a strong requirement for high EF in 3D biomimetic substrates. Moreover, the novel substrate was successfully applied in label-free animal virus detection and differentiation, and it exhibited potential as an effective SERS platform for cheap, rapid, sensitive, and reliable biochemical detection and sensing.

MATERIALS AND METHODS

Fabrication of Substrates. All of the cicadas are purchased at a strikingly low price ($0.1/cicada) from a coherent orchardist in Jiangsu Province of China. The fabrication process for the 3D biomimetic SERS substrate is shown in Figure 1. First, the cicada wings were ultrasonically cleaned with ultrapure water (18.25 MΩ cm) for 5 min to remove residue on the surface followed by drying in air and segmenting into 5×4 mm^2 sections using scissors and scalpel to exclude untextured venation. Next, the pretreated sections were fixed as bioscaffolds on glass slides with double-sided adhesive tape using tweezers. Finally, the as-prepared bioscaffolds were decorated with Ag NPs by sputtering Ag at a low ratio about 3.6 nm min^{-1} in a protective atmosphere of argon gas at room temperature. Ion sputtering was applied using an ETD-3000 (Beijing Elaborate Technology Development Ltd., $6000) ion sputter to decorate Ag NPs onto the surface of the CNAs. The sputtering was operated for different periods of duration with 4 mA ion current under 10 Pa argon gas (99.999%) pressure. In our experiments, every sputtering period consisted of a 1 min working duration coupled with a 1 min break. High-purity (99.99%) Au and Ag targets were sputtered under the same conditions. Two-dimensional Au-capped CNAs were fabricated by 16 min Au sputtering, whereas 2D Ag-capped CNAs were fabricated by 2 min Au sputtering followed by 12 min Ag sputtering. Unless otherwise stated, 3D biomimetic SERS substrates refers to CNAs with 14 Ag min sputtering. Gold-coated commercial Klarite SERS substrates were purchased from D3 Technologies Ltd. (Hampshire, UK).

Characterization. The CNAs on the cicada wing and 3D biomimetic SERS substrates were characterized by using field-emission scanning electron microscopy (FE-SEM, JSM-6700F, Japan). High-resolution transmission electron microscopy (HRTEM) images were obtained using a JEM-2010FEF microscope (JEOL, Japan). FTIR spectra were collected on a Nicolet Avatar-330 spectrometer (Thermo Nicolet, USA) with 4 cm^{-1} resolution using the KBr pellet technique. All Raman spectra were recorded at room temperature using an inVia Raman spectrometer (Renishaw, UK) equipped with a confocal microscope (Leica, German). The samples were excited with an Ar^+ laser (514.5 nm), a He−Ne laser (633 nm), or a diode laser (785 nm) for corresponding characterization with an output power of 1.5, 1.0, and 25.0 mW, respectively. The band of a silicon wafer at 520 cm^{-1} was used to calibrate the spectrometer. Unless otherwise stated, the SERS spectra were obtained with a 50× objective lens, 10 s exposure, and one time accumulation. Reflection spectra were recorded from ultraviolet-visible diffuse reflectance spectroscopy (Shimadzu UV-2550, Japan), with a smooth gold surface defined as a 100% reflection mirror for reference.

Calculation of the Average Enhancement Factor. The average enhancement factor (EF_{ave}) for the 3D biomimetic substrate was calculated using the accepted formula from the literature[51,52]

$$EF_{ave} = \frac{I_{SERS}/N_{SERS}}{I_{Bulk}/N_{Bulk}} = \left(\frac{H\rho}{R\mu}\right)\left(\frac{I_{SERS}}{I_{Bulk}}\right)$$

where I_{SERS} and I_{Bulk} are the intensities of the 1578 cm^{-1} peak in the SERS spectra and the 1583 cm^{-1} peak in bulk liquid Raman spectra, respectively. N_{SERS} and N_{Bulk} are the estimated numbers of benzenethiol (BT) molecules in the laser spot for the SERS substrates and neat reference sample, respectively. $N_{SERS} = AR\mu$ is the number of monolayer BT molecules absorbed on the substrates and contributes to the SERS signal, $N_{Bulk} = AH\rho$ is the number of BT molecules in bulk solution contributing to the unenhanced Raman signal. A is the area of the laser spot, R is the area factor, μ is the monolayer density of BT molecules on the Au and Ag substrate, ρ is the molecular density of neat BT solution, and H is the efficient collection height of the BT liquid layer that emits a Raman signal.

Herein, R is an intrinsic parameter of a substrate that defines the increased effective SERS-active area ratio by the following equation

$$R = \frac{S_{SERS}}{A_{beam}}$$

where S_{SERS} is the surface area of SERS-active sites under laser illumination and A_{beam} is the area of the flat detection beam. For the 50× objective lens used in our experiment, the detection-beam diameter is approximately 2.0 μm and the surface area of the beam is about 3.14 μm^2.

For the Klarite substrate, these SERS-active surfaces comprise gold-capped grids of pyramidal wells with a 2 μm × 2 μm aperture and ~2 μm depth.[53] Therefore, the effective SERS-active surface area is calculated to be about a 2.2-fold increase over the simple flat area of the excitation beam, namely, $R_{klarite} = 2.2$.

For 2D Ag-capped and 2D Au-capped CNAs, we followed the estimation approach described by Oh et al.[21] After sputter coating, the average height and diameter of the chitin nanopillars is 230 and 100

nm (Figure 2), respectively. SEM results indicate that there are 110−120 chitin nanopillars within a laser spot. By taking the side surfaces of the Ag- or Au-coated chitin nanopillars into consideration, the effective SERS-active surface area is about a 2.8-fold increase over the simple flat area of the excitation beam, namely, R_{2D} = 2.8.

For 3D Ag-decorated CNAs, a similar estimation approach was adopted. As stated above, there are approximately 1000 small Ag NPs with an average diameter of 40 nm and 100 big Ag NPs with an average diameter of 60 nm within 1 μm^2 unit after Ag sputtering. Meanwhile, the original chitin nanopillar is assumed to be a cone of 180 nm in height and 120 nm in basal diameter. Consequently, the total effective SERS-active surface area is estimated to be about a 3.0-fold increase over the simple flat area of the excitation beam, namely, R_{3D} = 3.0.

To estimate the molecule number illuminated in the normal Raman characterization, we followed the approach described by Cai et al.,[54] with the detection volume being defined as the volume of a hypothetical cylinder. For the 50× microscope lens that we chose, the confocal length H = 21 μm was used to calculate the detection volume. The μ and ρ values of BT are reported to be 3.3×10^{14} molecules/cm^2 and 5.9×10^{21} molecules/cm^3, respectively, in the literature.[55] The values of I_{SERS} and I_{Bulk} of BT were measured from different substrates under normalized experimental settings with the three common exciting laser lines being 514, 633, and 785 nm. For each laser excitation, SERS and bulk Raman measurements were conducted under identical experimental conditions (laser wavelength, laser power, and microscope objective lens). The SERS intensity is the average value of 30 measurements, and the Raman intensity is the average value of three measurements.

Preparation of Virus. All animal virus strains, PCV2 (gi: 225322671), PRV (Bartha-K61), and H5N1 (A/chicken/HuBei/327/2004), were acquired from the State Key Laboratory of Agricultural Microbiology of Huazhong Agricultural University. The virus samples were propagated and purified following routine procedures as described previously.[31−34] The concentrations of the three purified virus samples were about 1×10^6 PFU/mL, as tested by immunostaining plaque assay. Virus solutions of different concentrations were prepared by dilution with ultrapure water. All viruses were stored at −80°C before Raman test. In a typical experiment, a 1.0 μL sample of intact virus was applied to the 3D biomimetic SERS substrate and allowed to bind for 1 h at room temperature prior to spectrum acquisition. All SERS spectra of viruses were collected from multiple spots across the substrates.

■ ASSOCIATED CONTENT

Supporting Information

Photograph, HRTEM images, and stability of the 3D biomimetic SERS substrate; nanostructures of the cicada wing; dc sputtering effects with different deposition conditions; FTIR spectra of the cicada wing and the 3D biomimetic substrate; and multiple SERS spectra of the PCV2, PRV, and H5N1 from the 3D biomimetic substrates. This material is available free of charge via the Internet at http://pubs.acs.org.

■ AUTHOR INFORMATION

Corresponding Author

*Phone: +(86) 027-87280246. Fax: +(86) 027-87280246. E-mail: hyhan@mail.hzau.edu.cn.

Notes

The authors declare no competing financial interest.

■ ACKNOWLEDGMENTS

We gratefully acknowledge funding support for this research from the National Natural Science Foundation of China (21175051), the Natural Science Foundation of Hubei Province Innovation Team (2011CDA115), and the Fundamental Research Funds for the Central Universities (2012SC04 and 2013SC17). We also thank Beijing Myscimage Multimedia Technology Center for help with the art work.

■ REFERENCES

(1) Kneipp, K.; Kneipp, H.; Deinum, G.; Itzkan, I.; Dasari, R. R.; Feld, M. S. *Appl. Spectrosc.* **1998**, *52*, 175−178.
(2) Guerrini, L.; Graham, D. *Chem. Soc. Rev.* **2012**, *41*, 7085−7107.
(3) Tsoutsi, D.; Montenegro, J. M.; Dommershausen, F.; Koert, U.; Liz-Marzán, L. M.; Parak, W. J.; Alvarez-Puebla, R. A. *ACS Nano* **2011**, *5*, 7539−7546.
(4) Zavaleta, C. L.; Smith, B. R.; Walton, I.; Doering, W.; Davis, G.; Shojaei, B.; Natan, M. J.; Gambhir, S. S. *Proc. Natl. Acad. Sci. U.S.A.* **2009**, *106*, 13511−13516.
(5) Cao, Y. C.; Jin, R.; Mirkin, C. A. *Science* **2002**, *297*, 1536−1540.
(6) Ward, D. R.; Grady, N. K.; Levin, C. S.; Halas, N. J.; Wu, Y.; Nordlander, P.; Natelson, D. *Nano Lett.* **2007**, *7*, 1396−1400.
(7) Lee, S.; Hahm, M. G.; Vajtai, R.; Hashim, D. P.; Thurakitseree, T.; Chipara, A. C.; Ajayan, P. M.; Hafner, J. H. *Adv. Mater.* **2012**, *24*, 5261−5266.
(8) Xu, X.; Kim, K.; Li, H.; Fan, D. L. *Adv. Mater.* **2012**, *24*, 5457−5463.
(9) Haynes, C. L.; Van Duyne, R. P. *J. Phys. Chem. B* **2001**, *105*, 5599−5611.
(10) Dinish, U. S.; Yaw, F. C.; Agarwal, A.; Olivo, M. *Biosens. Bioelectron.* **2011**, *26*, 1987−1992.
(11) Tao, A.; Kim, F.; Hess, C.; Goldberger, J.; He, R.; Sun, Y.; Xia, Y.; Yang, P. *Nano Lett.* **2003**, *3*, 1229−1233.
(12) Wang, H.; Levin, C. S.; Halas, N. J. *J. Am. Chem. Soc.* **2005**, *127*, 14992−14993.
(13) Wang, H. H.; Liu, C. Y.; Wu, S. B.; Liu, N. W.; Peng, C. Y.; Chan, T. H.; Hsu, C. F.; Wang, J. K.; Wang, Y. L. *Adv. Mater.* **2006**, *18*, 491−495.
(14) Su, Q.; Ma, X.; Dong, J.; Jiang, C.; Qian, W. *Acs Appl. Mater. Inter.* **2011**, *3*, 1873−1879.
(15) Ko, H.; Singamaneni, S.; Tsukruk, V. V. *Small* **2008**, *4*, 1576−1599.
(16) Kodiyath, R.; Papadopoulos, T. A.; Wang, J.; Combs, Z. A.; Li, H.; Brown, R. J.; Brédas, J.-L.; Tsukruk, V. V. *J. Phys. Chem. C* **2012**, *116*, 13917−13927.
(17) Stoerzinger, K. A.; Hasan, W.; Lin, J. Y.; Robles, A.; Odom, T. W. *J. Phys. Chem. Lett.* **2010**, *1*, 1046−1050.
(18) Alvarez-Puebla, R. A.; Agarwal, A.; Manna, P.; Khanal, B. P.; Aldeanueva-Potel, P.; Carbo-Argibay, E.; Pazos-Perez, N.; Vigderman, L.; Zubarev, E. R.; Kotov, N. A.; Liz-Marzan, L. M. *Proc. Natl. Acad. Sci. U.S.A.* **2011**, *108*, 8157−8161.
(19) Ko, H.; Tsukruk, V. V. *Small* **2008**, *4*, 1980−1984.
(20) Kattumenu, R.; Lee, C. H.; Tian, L.; McConney, M. E.; Singamaneni, S. *J. Mater. Chem.* **2011**, *21*, 15218−15223.
(21) Oh, Y.-J.; Jeong, K.-H. *Adv. Mater.* **2012**, *24*, 2234−2237.
(22) Caldwell, J. D.; Glembocki, O.; Bezares, F. J.; Bassim, N. D.; Rendell, R. W.; Feygelson, M.; Ukaegbu, M.; Kasica, R.; Shirey, L.; Hosten, C. *ACS Nano* **2011**, *5*, 4046−4055.
(23) Tang, H.; Meng, G.; Huang, Q.; Zhang, Z.; Huang, Z.; Zhu, C. *Adv. Funct. Mater.* **2012**, *22*, 218−224.
(24) Tan, E.-Z.; Yin, P.-G.; You, T.-t.; Wang, H.; Guo, L. *ACS Appl. Mater. Interfaces* **2012**, *4*, 3432−3437.
(25) Dawson, P.; Duenas, J. A.; Boyle, M. G.; Doherty, M. D.; Bell, S. E. J.; Kern, A. M.; Martin, O. J. F.; Teh, A. S.; Teo, K. B. K.; Milne, W. I. *Nano Lett.* **2011**, *11*, 365−371.
(26) Stoddart, P. R.; Cadusch, P. J.; Boyce, T. M.; Erasmus, R. M.; Comins, J. D. *Nanotechnology* **2006**, *17*, 680−686.
(27) Garrett, N. L.; Vukusic, P.; Ogrin, F.; Sirotkin, E.; Winlove, C. P.; Moger, J. *J. Biophotonics* **2009**, *2*, 157−166.
(28) Kostovski, G.; White, D. J.; Mitchell, A.; Austin, M. W.; Stoddart, P. R. *Biosens. Bioelectron.* **2009**, *24*, 1531−5.
(29) Huang, Z.; Meng, G.; Huang, Q.; Yang, Y.; Zhu, C.; Tang, C. *Adv. Mater.* **2010**, *22*, 4136−4139.
(30) Schmidt, M. S.; Hübner, J.; Boisen, A. *Adv. Mater.* **2012**, *24*, OP11−OP18.

(31) Winau, D.; Koch, R.; Weber, M.; Rieder, K.; x; H; Garg, R. K.; Schurig, T.; Koch, H. *Appl. Phys. Lett.* **1992**, *61*, 279−281.
(32) Campbell, C. T. *Surf. Sci. Rep.* **1997**, *27*, 1−111.
(33) Im, H.; Bantz, K. C.; Lindquist, N. C.; Haynes, C. L.; Oh, S. H. *Nano Lett.* **2010**, *10*, 2231−2236.
(34) Cho, W. J.; Kim, Y.; Kim, J. K. *ACS Nano* **2012**, *6*, 249−255.
(35) Tan, Y.; Gu, J.; Zang, X.; Xu, W.; Shi, K.; Xu, L.; Zhang, D. *Angew. Chem., Int.. Ed.* **2011**, *50*, 8307−8311.
(36) Kaminska, A.; Dziecielewski, I.; Weyher, J. L.; Waluk, J.; Gawinkowski, S.; Sashuk, V.; Fialkowski, M.; Sawicka, M.; Suski, T.; Porowski, S.; Holyst, R. *J. Mater. Chem.* **2011**, *21*, 8662−8669.
(37) Choi, D.; Choi, Y.; Hong, S.; Kang, T.; Lee, L. P. *Small* **2010**, *6*, 1741−1744.
(38) Xu, J.; Kvasnička, P.; Idso, M.; Jordan, R. W.; Gong, H.; Homola, J.; Yu, Q. *Opt. Express* **2011**, *19*, 20493−20505.
(39) Wu, H.-Y.; Choi, C. J.; Cunningham, B. T. *Small* **2012**, 2878−2885.
(40) Cheng, S.; Zhang, M.; Li, W.; Wang, Y.; Liu, Y.; He, Q. *J. Proteomics* **2012**, *75*, 3258−3269.
(41) Qiu, H.-J.; Tian, Z.-J.; Tong, G.-Z.; Zhou, Y.-J.; Ni, J.-Q.; Luo, Y.-Z.; Cai, X.-H. *Vet. Immunol. Immunopathol.* **2005**, *106*, 309−319.
(42) Huang, H.; Dan, H.; Zhou, Y.; Yu, Z.; Fan, H.; Tong, T.; Jin, M.; Chen, H. *Mol. Immunol.* **2007**, *44*, 1052−1055.
(43) Li, X.; Lu, D.; Sheng, Z.; Chen, K.; Guo, X.; Jin, M.; Han, H. *Talanta* **2012**, *100*, 1−6.
(44) Madson, D.; Patterson, A.; Ramamoorthy, S.; Pal, N.; Meng, X.; Opriessnig, T. *Theriogenology* **2009**, *72*, 747−754.
(45) Nauwynck, H.; Glorieux, S.; Favoreel, H.; Pensaert, M. *Vet. Res.* **2007**, *38*, 229−241.
(46) Webster, R. G.; Bean, W. J.; Gorman, O. T.; Chambers, T. M.; Kawaoka, Y. *Microbiol. Rev.* **1992**, *56*, 152−179.
(47) He, Q.; Velumani, S.; Du, Q.; Lim, C. W.; Ng, F. K.; Donis, R.; Kwang, J. *Clin. Vaccine Immunol.* **2007**, *14*, 617−623.
(48) Chen, L.; Sheng, Z.; Zhang, A.; Guo, X.; Li, J.; Han, H.; Jin, M. *Luminescence* **2010**, *25*, 419−423.
(49) Shanmukh, S.; Jones, L.; Driskell, J.; Zhao, Y.; Dluhy, R.; Tripp, R. A. *Nano Lett.* **2006**, *6*, 2630−2636.
(50) Němeček, D.; Thomas, G. J. In *Digital Encyclopedia of Applied Physics*; Trigg, G. L., Ed.; Wiley-VCH: New York, 2009; Chapter 13, p 423.
(51) Yap, F. L.; Thoniyot, P.; Krishnan, S.; Krishnamoorthy, S. *ACS Nano* **2012**, *6*, 2056−2070.
(52) Fu, C. Y.; Kho, K. W.; Dinish, U.; Koh, Z. Y.; Malini, O. *J. Raman Spectrosc.* **2012**, *43*, 977−985.
(53) Kantarovich, K.; Tsarfati, I.; Gheber, L. A.; Haupt, K.; Bar, I. *Biosens. Bioelectron.* **2010**, *26*, 809−814.
(54) Cai, W. B.; Ren, B.; Li, X. Q.; She, C. X.; Liu, F. M.; Cai, X. W.; Tian, Z. Q. *Surf. Sci.* **1998**, *406*, 9−22.
(55) Fang, Y.; Seong, N.-H.; Dlott, D. D. *Science* **2008**, *321*, 388−392.